OLAF: a Swarm of SmallSats for Active Debris Removal by Space-based Laser Ablation

Andrei-Gabriel Pavel[(1)], Anthonius Daoud-Moraru[(1)], Constantin Alexandru Pandele[(1)], Dan Șelaru[(1)], Ionuț-Robert Miron[(1)], Ileana Mihu[(1)], Sergiu-Ștefan Mihai[(1)], José Antonio Garcia-Molina[(2)]

[(1)]Romanian InSpace Engineering S.R.L.
Bucharest, Romania
Email: andrei.pavel@roinspace.com

[(2)]European Space Agency (ESA)
Noordwijk, The Netherlands
Email: jose.antonio.garcia.molina@esa.int

Abstract—**Small debris objects (1 mm–10 cm) pose a considerable risk to active spacecraft, potentially causing mission-critical damage as they can reach relative impact velocities of 15 km/s in LEO. ESA's latest Space Environment Report estimates more than 140 million objects in this size range residing in LEO, the majority of which cannot be tracked by current ground-based space surveillance systems due to their small size.**

OLAF (Orbital Laser Ablation Formation) is a proposed mission concept that employs a swarm of 8 small satellites (1 chief and 7 deputies) working together to detect, track, and remove small debris fragments from low Earth orbits using space-based laser ablation. The chief spacecraft is equipped with a wide-FOV 40-cm f/1.2 telescope for debris detection and coarse trajectory estimation. The deputies carry high-resolution, narrow-FOV 60-cm f/3.25 telescopes for precision tracking. In addition, the deputies are equipped with high-power 6.0 kW pulsed Nd:YAG lasers operating at 355 nm, whose combined fluence at the target exceeds the ablation threshold, thus effectively decelerating approaching debris objects and reducing their orbital lifetime. Laser-debris interactions were simulated for various impact geometries, yielding significant lifetime reductions for fragments approaching from altitude differences of up to 10 km and azimuth angle differences of up to 40 degrees.

The project focused on the autonomous navigation and formation-flying aspects of the mission. The swarm activities are coordinated by the chief spacecraft, which receives GNSS-based PVT and RF ranging data from the deputies via the inter-satellite link, and processes them using an Extended Kalman Filter to estimate the relative states of the swarm. A formation keeping strategy is proposed, with simulations indicating that each deputy requires an annual ΔV between 48 and 187 m/s. The mission's economic aspects are discussed, with the system capable of deorbiting 130,000 small debris objects over 5 years, at an estimated cost of €3500 per object.

Keywords—space debris, laser ablation, formation flying

I. INTRODUCTION

Since the launch of Sputnik 1 in 1957, the space debris population has increased continuously with the ever-growing number of artificial objects launched in Earth orbit. Currently, there are roughly 45,000 objects tracked by space surveillance segments, of which 15,000 are active payloads, according to the latest Annual Space Environment Report by ESA [1]. However, the number of space debris objects inhabiting near-Earth orbits is much higher, since many of these are too small to reliably be tracked from the ground. As such, the 2024 reference population of the MASTER-8 statistical model released by ESA estimates that there are currently more than 1.2 million space debris objects in the 1 cm – 10 cm diameter range, and more than 140 million debris objects in the 1 mm – 1 cm range [2]. With the projected launch of satellite mega-constellations in the near future, the space debris population is expected to grow even further, increasing the probability of the collisional cascading effect theorised by Kessler and Cour-Palais [3].

Space debris objects consist of inactive spacecraft, spent rocket stages, fragments resulting from collisions or in-orbit break-ups, solid rocket motor slag and dust, paint flakes, NaK coolant droplets, MLI fragments, ejecta etc. [4]. Most of these reside in low Earth orbit (LEO), where the relative impact velocities with other space objects can reach 15 km/s. Such hypervelocity impacts pose a major threat to active spacecraft, as millimetre and centimetre-sized objects can puncture pressure vessels, walls, and cause critical structural or functional damage to the onboard systems [5].

To minimise this threat, mitigation measures have been developed, including End-of-Life disposal of spacecraft, passivation of stored energy sources, enhanced systems resilience and monitoring, and improved collision avoidance capabilities. However, a universal set of space debris mitigation requirements has been difficult to enforce internationally, and adherence to the various existing guidelines has been weak [6]. In particular, in 2023 ESA instated a stricter requirement regarding the maximum allowed disposal duration in LEO, reducing it from 25 to 5 years [7].

Alternatively, remediation strategies aim to reduce the debris population by removing existing objects. Active Debris Removal (ADR) concepts fall within this category. Various methods have been proposed: capturing mechanisms (robotic arms, tentacles, nets, grippers, harpoons), drag augmentation systems (foam-based, fiber-based), electro-dynamic tethers, contactless removal methods (lasers, ion-beam shepherds, artificial atmosphere generation) etc. [8]. However, most of these methods are only viable for the removal of individual, large debris, as they need to approach at close range or capture the object. A solution to remove large numbers of small debris objects that has been thoroughly explored in the literature is represented by laser systems (either ground-based or space-based), as they can impart momentum on debris objects from long distances in a contactless manner, without requiring manoeuvres to intercept them.

Although more difficult to develop, a space-based laser system could also target the population of small debris that

*This project was funded by ESA under the NAVISP Element 1 programme, which supports the development of innovative PNT technologies, systems, and services.

are untrackable from the ground (1 mm – 10 cm) by detecting them 'in situ'. As such, it is one of the only feasible solutions for the remediation of this population. The idea of deorbiting debris objects using space-based laser ablation was first proposed by Schall in 1991 [9]. Since then, various other studies have further developed the concept and provided mission-level feasibility analyses.

Phipps [10] proposed L'ADROIT, a 10,000-kg system capable of firing 21-kW laser bursts (with 380 J pulses at 56 Hz repetition frequency), requiring a solar array area of 247 m^2 and a primary mirror diameter of 1.5 m. An approximate number of 100,000 objects could be removed at an estimated total cost of $560M. Pieters and Noomen [11] designed a 20-kW laser shooting 300 J pulses at a frequency of 66.66 Hz, using a 2.0-m mirror. They estimated that the lifetime of about 15,000 debris objects could be reduced to below one month, per year, using their system.

Bögel et al. [12] devised a 27.7-kW laser (firing 116 J pulses at 55.8 Hz frequency) with a 4.02-m primary mirror, which requires a 35 m^2 solar array, estimating a total mass of 2794 kg and a total mission cost of €550M. The aim was to de-orbit 50% of the debris generated by an on-orbit fragmentation event comparable to the 2009 Iridium-Cosmos collision. Walker and Vasile [13] conceived a more compact system, of 100-300 kg total mass, with a 54-kW pulsed laser (firing 3 kJ pulses at 18 Hz frequency), a 1.32-m aperture diameter, and a 10 m^2 solar array, recharging batteries of 4.62 kg in 22.8 minutes. They showed that a space-based laser ablation platform may be a feasible solution to remove debris created from satellite breakup events in LEO.

This work proposes an alternative to the large, monolithic platforms described in the literature, by introducing a swarm of SmallSats (300-500 kg class) which work together to perform debris removal in LEO by detecting and tracking small objects (1 mm – 10 cm in diameter) as they approach, focusing their laser beams on them and achieving the high fluences necessary for ablation and deceleration of the debris objects from large enough distances. By applying thrust approximately opposite to the debris object's velocity vector, its orbital energy is reduced, imparting a negative ΔV and thereby reducing its orbit lifetime. The objective is to add up the thrust imparted by each of the lasers on the object, and thus achieve a similar performance to that of a much larger individual spacecraft equipped with a more powerful laser system.

The main advantages that a swarm of SmallSats can bring over a single monolithic spacecraft consist of task distribution (e.g. detection, tracking, laser firing) between swarm members, allowing for smaller platforms and payload requirements, as well as a higher redundancy and robustness of the mission owing to the distributed system design. If critical failures can be mission-ending for a single monolithic spacecraft, a swarm can continue its operations even if one of the satellites becomes inactive, albeit at reduced performance. In such a case, only part of the swarm needs to be replaced, as opposed to the entire mission.

To the authors' knowledge, the only study in the literature outlining a distributed formation of smaller satellites for space-based ADR by laser ablation is Fodde et al. [14], in which they proposed a swarm of 28 CubeSats to place the 365-kg NASA ATS-3 satellite to a graveyard orbit 300 km above the GEO protected region. This work tackles the problem of small debris objects in LEO.

II. System Description

A. Configuration of the satellite swarm

A circular formation of 7 satellites actively uses its lasers to ablate and decelerate the debris object. Each of them is equipped with a narrow-FOV steerable Cassegrain telescope and a high-resolution detector array for continuous tracking of the target, in addition to an active firing unit consisting of a pulsed Nd:YAG solid-state laser. The mirror system of the telescope focuses the laser beam at the desired ranges. A beam splitter is used to separate the incident light beam coming from the debris object from the transmitted laser pulses.

One chief spacecraft (placed at the centre) coordinates the activity of the entire swarm. The chief receives GNSS-based PVT information and RF ranging measurements from the deputy satellites via the inter-satellite link (ISL), and uses a sensor fusion algorithm to compute the relative states of the swarm. This way, the chief can detect if there is a high collision risk between any two satellites, and autonomously compute the required collision avoidance manoeuvre, which is then sent via the ISL. Moreover, the chief provides direct communication with the ground to establish the TT&C (Telemetry, Tracking & Command) link.

The chief spacecraft also houses the passive, wide-FOV debris detection optical sensor. This is a non-steerable optical telescope, which can detect small debris objects passing through its FOV, otherwise untrackable from the ground. Its wide FOV comes at the cost of resolution, therefore it can only send coarse debris position and trajectory information to the laser satellites. Subsequently, these point their high spatial resolution tracking instrument towards the estimated position, and refine their pointing until they follow the precise orbital track computed, such that the laser spot is focused and fixed on the debris.

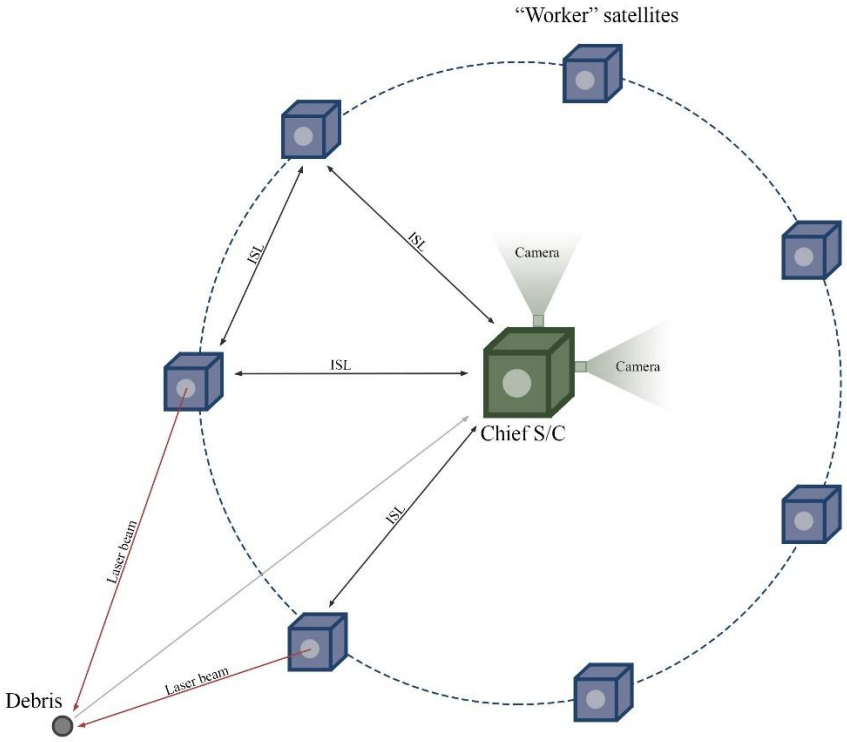

Figure 1. Configuration of the circular formation of satellites, with the chief at the centre.

B. Detection and tracking systems

a) Detection telescope

The detection sensor is a 40-cm f/1.2 telescope, spanning a wide 40° FOV. The detector is composed of a 4096x4096-pixel array, with 82 µm pixel size, reaching a physical dimension for the detector of 33.6 cm. The image scale is 35.24 arcseconds/pixel, resulting in a best-case (not accounting for orbit determination covariances) positioning uncertainty of 34 m for a debris object at 200 km distance. With a 10-ms exposure time, a 1-cm debris object can be detected from 487 km away.

This sensor remains in a fixed position (non-steerable), and scans the sky for opportunistic debris encounters. It can therefore detect debris objects that are untrackable from the ground, and provide coarse position and trajectory information that is sent to the deputy satellites, which then rotate their steerable tracking telescopes to the estimated position for further refining.

b) Tracking telescopes

The tracking sensors are 60-cm f/3.25 Cassegrain telescopes, with a narrow FOV of only 3.6 arcmin. The detector is a 2048x2048 pixel array, with 1 µm pixel size, reaching a physical size for the detector array of 2.05 mm. The image scale is thus 0.11 arcsec/pixel, resulting in a spatial resolution of 10 cm at 200 km range, which is the expected distance at which the ablation threshold is exceeded. With a 5-ms exposure, a debris object of 1 cm in diameter can be observed from 465 km away.

Once the sensor is stabilized, laser pulses are sent towards the debris object. The laser's pointing direction is optimised and its focus adjusted until the spot reaches the desired diameter at the debris. Agile, variable-focus optics are required to track debris objects longitudinally with the focal plane of the beam [13]. Range information is thus necessary to achieve this. It can be obtained by measuring the time interval for the returning laser photons, reflected back by the debris object's surface (these should increase the image SNR by a predictable amount). When the blue flash of plasma is observed at the target, the beginning of the ablation process is confirmed [10].

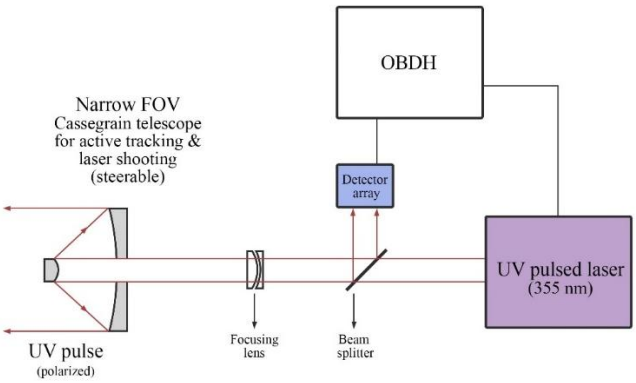

Figure 2. Schematic diagram of the active tracking and laser shooting system.

c) SNR analysis

A signal-to-noise ratio (SNR) analysis was performed to estimate the telescopes' performance. From first principles, the signal in the central pixel is:

$$S = \frac{\Phi_{\odot_{vis.}} \cdot A_{deb.} \cdot \alpha_{deb.} \cdot A_{tel.} \cdot \Delta t \cdot QE}{2\pi r^2 \cdot E_{ph.} \cdot n_{pixels}} \quad (1)$$

where $\Phi_{\odot_{vis.}}$ is the solar spectral irradiance in the visible spectrum (~39% of the total irradiance, 1372.3 $\frac{W}{m^2}$ at 1 AU [15]), $A_{deb.}$ is the illuminated surface area of the spherical debris object, $\alpha_{deb.}$ is the albedo of the debris object, $A_{tel.}$ is the light collecting area of the telescope, Δt is the integration time, QE is the quantum efficiency of the detector, r is the telescope-debris distance, $E_{ph.}$ is the mean energy of a photon at 502 nm, n_{pixels} is the number of pixels across which the object image is spread on the detector array. The factor $1/2\pi r^2$ assumes isotropic reflection of sunlight by the spherical debris object across one hemisphere.

The total noise per pixel can be estimated by [16]:

$$\sigma_N = \sqrt{\sigma_B^2 + \sigma_S^2 + \sigma_D^2 + \sigma_R^2} \quad (2)$$

where $\sigma_S = \sqrt{S}$ is the Poisson object noise, $\sigma_B = \sqrt{B}$ is the sky background noise (assumed as 21 mag/arcsec^2), σ_R is the readout noise generated in the detector (assumed as 10 electrons/ exposure/ pixel); $\sigma_{D\,=}\sqrt{D}$ is the dark current noise (dark current D assumed as 100 electrons/second/pixel, mentioning that that the CCDs shall need to be actively cooled to -20° C or below during acquisition for optimal performance).

We regard a signal-to-noise ratio (SNR) of 3 as a marginal detection of an object. The SNR results are presented below.

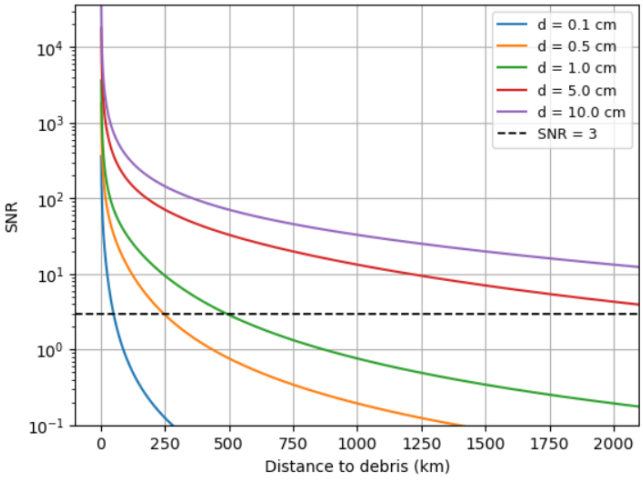

Figure 3. SNR vs. distance for different debris diameters. For the 40-cm f/1.2 detection telescope. Exposure time = 10 ms.

Debris diameter (cm)	Detection distance (km)
0.1	48.7
0.5	243.5
1	487.1
5	2435.0
10	4871.0

Table 1. Distances from which small debris objects of various sizes can be detected by the 40-cm f/1.2 telescope. Exposure time = 10 ms.

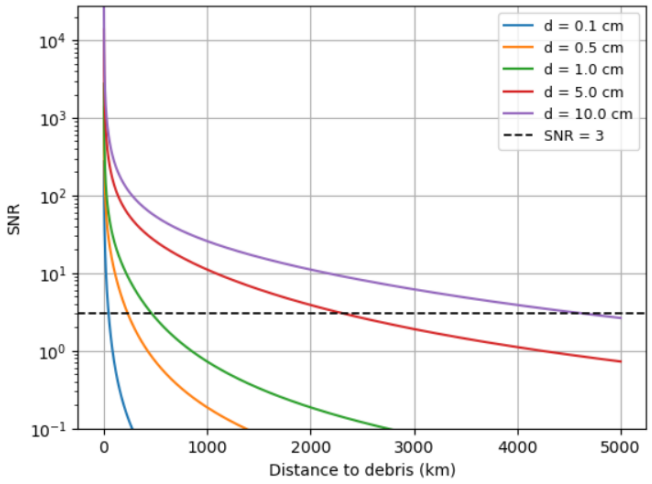

Figure 4. SNR vs. distance for different debris diameters. For the 60-cm f/3.25 tracking telescope. Exposure time = 5 ms.

Debris diameter (cm)	Detection distance (km)
0.1	46.5
0.5	232.7
1	465.4
5	2327.3
10	4654.6

Table 2. Distances from which small debris objects of various sizes can be tracked by the 60-cm f/3.25 telescope. Using a 5-ms exposure time.

C. *Laser system*

a) Description

A pulsed Nd:YAG solid state laser operating at the third harmonic, λ = 355 nm, is used on board each of the deputy satellites to ablate the approaching debris object. The table below lists the set of parameters describing the chosen laser system.

Parameter	Description	Value
$P_{laser,opt.}$	Optical power of the laser	6.0 kW
$\eta_{electr.\ to\ opt.}$	Electrical-to-optical efficiency	0.32
$P_{electr.,tot.}$	Total electrical power required by laser	18.75 kW
E_{pulse}	Laser pulse energy	80 J
f_{pulse}	Pulse frequency	75 Hz
D	Aperture diameter of primary mirror	0.6 m
D_{eff}	Effective exit beam diameter	0.54 m
λ	Laser wavelength	355 nm
M^2	Laser beam quality	2.0
a	Constant due to diffraction	1.27

T_{eff}	Transmission efficiency factor	0.9
τ	Pulse duration	100 ps

Table 3. Laser system - main parameters.

The optical power required by the pulsed laser is:

$$P_{laser} = E_{pulse} \cdot f_{pulse} \quad (3)$$

The laser fluence is the energy delivered by the laser beam per unit area of the targeted material [10]:

$$\Phi = \frac{4\, E_{pulse}\, D_{eff}^2\, T_{eff}}{\pi\, M^4\, a^2\, \lambda^2\, d_{rel}^2} \qquad [J/m^2] \quad (4)$$

Here, E_{pulse} is the energy of a pulse, D_{eff} is the effective aperture diameter of the mirror, and d_{rel} is the relative distance between laser and debris. T_{eff} is a factor quantifying the efficiency of energy transmission from aperture to the target, accounting for all system losses (e.g. apodization, obscuration [10]). λ is the wavelength of the light beam, M^2 is the beam quality factor (i.e. the inverse of the Strehl ratio: $M^2 = \frac{1}{S}$), and a is a constant regulating diffraction. Assuming a Gaussian intensity profile with $M^2 = 2$, we obtain $a = 1.27$ and D_{eff} is 90% of the total diameter of the mirror [17].

When this fluence Φ exceeds a certain threshold, depending on the material, ablation occurs. First, the targeted material is removed by thermal evaporation. Then, as the fluence continues increasing, a plasma jet is formed, being ejected away from the surface of the debris. This, in turn, generates a thrust in the opposite direction, decelerating the approaching debris object.

The acceleration imparted on the debris object as a consequence of the ablation process is:

$$a_{debris} = \frac{F_{thrust}}{m} = \Phi \cdot \left(\frac{A}{m}\right) \cdot C_m \cdot f_{pulse} \quad (5)$$

Here, $\left(\frac{A}{m}\right)$ is the area-to-mass ratio of the debris object, C_m is the momentum coupling coefficient, and f_{pulse} is the frequency of the laser pulses.

Finally, the Delta-V applied to the target can be computed as:

$$\Delta v = \int_{t_0}^{t_{end}} a_{debris}(t)\, dt \quad (6)$$

b) Momentum coupling coefficient

The key parameter modulating the acceleration is the momentum coupling coefficient, C_m, which quantifies the effectiveness of generating momentum via the ablation process. It is defined as the ratio of momentum transferred to the incident laser energy: $C_m = \frac{p}{E}$. It depends on a number of factors, including the material being ablated, the intensity of the beam I, the wavelength λ, as well as the pulse duration τ: $C_m = \frac{C_{m,0}}{(I\lambda\sqrt{\tau})^{\frac{1}{4}}}$, where $C_{m,0}$ is a material-dependent value [17].

When ablation begins, the material is vaporised by the high energy density of the laser. There is a sharp increase in the C_m vs. fluence curve, until a maximum is reached at the vapour-plasma transition. This is when the optimum fluence Φ_{opt} has been reached. As the fluence keeps increasing, C_m starts decreasing, more slowly than it has reached the top, due to a phenomenon called plasma shielding [18]. The plasma jet generated starts absorbing the incoming radiation, suppressing further material evaporation.

In this work, we used the empirical model for the momentum coupling coefficient devised by Tsuno et al. [19]. This was based on their experiment in which they investigated the impulse generated by an Nd:YAG laser irradiating a sample of A7075 aluminium alloy:

$$C_m = \begin{cases} 0, & if\ \Phi < \Phi_{th} \\ \dfrac{S_m(\Phi - \Phi_{th})}{\Phi}, & if\ \Phi_{th} \le \Phi \le \Phi_{max} \\ 0, & if\ \Phi > \Phi_{max} \end{cases} \quad (7)$$

where Φ is the irradiation fluence, Φ_{th} is the ablation fluence (minimum) threshold, Φ_{max} is the maximum fluence (before plasma shielding takes over), and S_m is the momentum coupling slope coefficient.

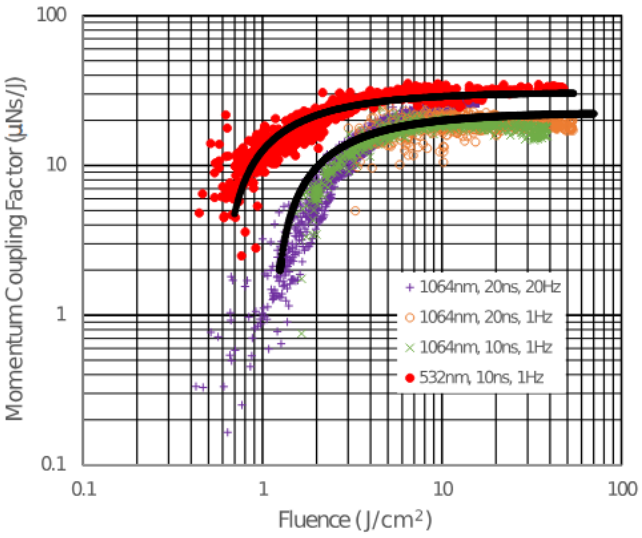

Figure 5. Measured momentum coupling coefficients as a function of fluence. For the Nd:YAG fundamental (1064 nm) and second harmonic (532 nm), and A7075 Aluminium alloy as a target. Taken from [19].

They found that there is a lower fluence at which ablation begins, as well as a higher momentum coupling coefficient for the second harmonic of Nd:YAG lasers, at 532 nm. The trend should continue for lower wavelengths. However, to the authors' knowledge, there have been no similar experiments investigating the coupling coefficient for the third harmonic, at 355 nm. Therefore, for the 355 nm laser, we adopted the same values that Tsuno et al. [19] obtained for 532 nm, noting that this is a conservative estimate:

- $\Phi_{th} = 6\,\frac{kJ}{m^2}$;
- $S_m = 31\,\frac{N}{MW}$;
- $\Phi_{max} = 500\,\frac{kJ}{m^2}$.

Using this model, a maximum momentum coupling coefficient for Aluminium of $C_m = 30.6 \frac{N}{MW}$ is obtained, consistent with the literature.

c) Beam spot diameter

For the energy density on the target to be maximised, the optical system needs to be designed such that the focal plane is placed at the distance where the target is found. Since the laser-debris interaction is a dynamic encounter, the beam waist plane must be aligned longitudinally with the direction of the incoming object, and variable focus optics must shift the focal plane such that the laser is always focused on the target, as the distance between the two objects decreases [13].

The beam spot radius at the focal plane is equal to [17]:

$$r_0 = \frac{2M^2 \lambda d_{rel}}{\pi D} \quad (8)$$

, in the limit $d_{rel} \gg D$.

With our chosen system, the beam spot diameter is equal to 33.5 cm at 200 km range (the furthest distance at which ablation starts occurring), and 3.35 cm at 20 km range (the closest distance at which ablation can still occur).

III. Modelling of Debris Removal by Laser Ablation

A. Modelling approach

The approach was to simulate the interaction between the laser and an individual debris object, testing the geometries under which a significant reduction in the orbital lifetime of the debris can be achieved. Similarly to [11], our method focused on the geometric nature of the problem, as debris objects can impact a spacecraft from various azimuth and elevation angles.

The simulations were performed using a custom orbital propagator, validated with the high-precision orbital propagator from STK. The equations of motion were integrated using a Runge-Kutta method of order 8, and the following perturbations were implemented in the propagator: Earth's gravitational potential, corresponding to a zonal spherical harmonic model up to the 6th order, third-body perturbations from the Sun and the Moon's gravitational influence, atmospheric drag corresponding to the Jacchia-Roberts 1971 density model [20], solar radiation pressure (SRP), including shadowing effects.

a) Initial states

All objects are initialized on the 1st of January 2030, at 00:00 UTC. The initial state of the laser satellite is given by the orbit described in the table below. It is a dawn/dusk Sun-synchronous orbit at 800 km altitude, in one of the LEO regions with the highest spatial densities of space debris [2]. Such a dawn/dusk orbit ensures nearly permanent sunlight, offering constant illumination conditions to the optical system responsible for detecting debris objects against other stellar objects in the background.

Orbital parameter	Value
Semi-major axis (a)	7178 km
Eccentricity (e)	0
Inclination (i)	98°
Argument of periapsis (ω)	0°
RAAN (Ω)	0°
True anomaly (v)	358°

Table 4. Laser satellite initial orbit parameters.

For the debris to encounter the laser, it must be placed on the same orbit, but moving in the opposite direction. This can be achieved by setting the inclination to $i_{debris} = 180° - i_{laser}$, the argument of periapsis to $\omega_{debris} - \omega_{laser} = 180°$, and the RAAN to $\Omega_{debris} - \Omega_{laser} = 180°$.

Orbital parameter	Value
Semi-major axis (a)	7178 km ± Δr
Eccentricity (e)	0
Inclination (i)	82° ± $\Delta\varphi$
Argument of periapsis (ω)	180°
RAAN (Ω)	180°
True anomaly (v)	358°

Table 5. Configuration of the debris object initial orbital parameters, to ensure it impacts the laser satellite.

To test different geometries at the point of collision or closest approach, the altitude and/or the inclination of the debris object can be changed, by setting Δr and $\Delta\varphi$ to the desired values. In the head-on, coplanar collision, $\Delta r = \Delta\varphi = 0$.

The objects encounter each other at the equator, where the difference in inclination is equal to the difference in azimuth angle $\Delta\varphi$, i.e. the angle at which the laser targets the debris object [21].

b) Object description

The laser satellites in the swarm are modelled as presented in the table below.

Parameter	Laser satellite
Drag cross-sectional area (m^2)	1.35
SRP cross-sectional area (m^2)	1.2
Mass (kg)	500
Drag coefficient C_D	2.2
Reflectivity coefficient C_r	1.1

Table 6. Parameters modelled for the orbital propagation of the laser satellites.

The space debris objects are modelled using the following area-to-mass ratio values, extracted from [22]:

Diameter (cm)	0.1	0.2	0.5	1	5	10
AMR (m^2/kg)	0.8	0.5	0.3	0.16	0.07	0.04

Table 7. Modelled debris object characteristics, by diameter.

c) Ablation termination conditions

Using the method presented in [11], two conditions are employed and verified at each step in the integration. If either of these does not hold anymore, the ablation process is stopped.

First of all, the debris object must move towards the laser. If the debris is moving away from the laser, applying an acceleration along the laser-debris displacement vector will raise the orbital energy of the debris, raising its apogee and increasing its lifetime. This condition can be verified by computing the dot product of the relative velocity and relative position vector of the two objects: if $\mathbf{d_{rel}} \cdot \mathbf{v_{rel}} < 0$, the debris is moving towards the laser; else, it is moving away.

Second of all, the angular rate of the laser mirror's steering mechanism must not exceed 2°/s. As the debris moves towards the laser with relative velocity $\mathbf{v_{rel}}$, it will also move across the field of view of the observing sensor with transversal velocity v_{trans}. To track and maintain the laser beam focused on the target, the telescope must rotate with angular velocity ω, which can reach a maximum of 2°/s with state-of-the-art steering mechanisms [17]. Thus, the simulation will be stopped whenever this threshold is surpassed. This can happen at a closer or further distance of the debris with respect to the laser, depending on the geometry of the interaction.

An expression for $\boldsymbol{\omega}$ can be obtained from trigonometry. The angle between the relative distance and velocity vectors is given by:

$$\beta = \arccos\left(\frac{d_{rel} \cdot v_{rel}}{|d_{rel}| \cdot |v_{rel}|}\right) \quad (9)$$

The transversal velocity is the velocity component in the direction perpendicular to the relative position vector:

$$v_{trans} = v_{rel} \sin\beta \quad (10)$$

The angular velocity is thus:

$$\omega = \frac{v_{trans}}{d_{rel}} = \frac{v_{rel} \sin\beta}{d_{rel}} \quad (11)$$

In addition, the ablation process is stopped if the upper ablation threshold (from which plasma shielding is considered to occur) is reached before any of the above termination conditions are met.

d) Other key aspects

The laser satellite swarm is placed on an 801-km SSO at 98° inclination, i.e. 1 km above the nominal 800-km orbit, to eliminate the possibility of collisions between the laser satellites and targeted debris objects. In reality, it is unlikely that sufficient TCA (time of closest approach) separations can be achieved by ablation alone, hence the swarm should employ standard collision avoidance manoeuvres if an imminent collision risk is identified, prioritising this over the mission objectives of debris removal.

For the laser swarm, only one satellite is modelled, to reduce the computational load. The laser fluence on the target is then multiplied by 7, the number of active satellites in the swarm. An efficiency factor of 90% in the imparted thrust is used here. This is due to the geometry of the swarm members, to account for the varying angles at which the laser beams are incident on the debris object. This value is consistent with the formation keeping simulation results presented in the following sections.

Reaction times are considered, and estimated in the table below, illustrating the typical duration the system has available from initial detection of an object until it needs to start ablating it at a relative distance of ~195 km, when the ablation threshold is exceeded. A worst-case relative velocity of 15 km/s is assumed for the reaction times.

Debris diameter (cm)	Detection distance (km)	Tracking distance (km)	Reaction time (s)
0.1	48.7	46.5	0.00
0.2	97.4	93.0	0.00
0.5	243.5	232.7	2.51
1	487.1	465.4	18.03
5	2435.0	2327.3	142.15
10	4871.0	4654.6	297.31

Table 8. Detection distance, tracking distance, and reaction time for the system until ablation should begin at 195-km range.

B. Simulation results

Different lifetime reductions were obtained, based on the varying laser-debris interaction geometry. This refers both to the altitude and azimuth angle from which the debris object approaches.

According to ESA's MASTER model, on an 800-km SSO at 98° inclination, 70.7% of the objects impacting a spherical surface come from azimuth angles in the ±40° range, while 83.0% of the objects come from azimuths of ±60°. 49.3% of the impactors originate from the narrower ±20° azimuth range. Therefore, most objects expected to be encountered come head-on, with the flux distribution decreasing towards higher impact angles.

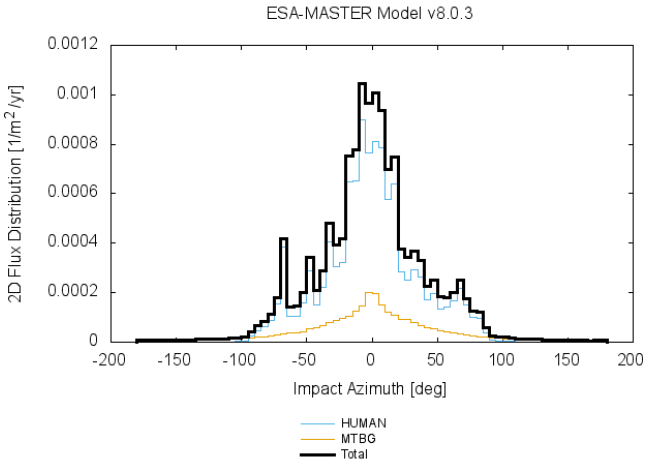

Figure 6. MASTER flux distribution for 0.1-10 cm debris objects impacting a spherical surface orbiting on an 800-km SSO at 98° inclination. 2D flux as a function of impact azimuth: 0° = head-on impact, 90°= edge-on/from the side, 180° = tail-on impact.

a) Debris objects at the baseline altitude

The first results reported below look at interactions with debris objects at the same altitude (i.e. the baseline 800 km) as the laser system. Five debris diameters were considered (2 mm, 5 mm, 1 cm, 5 cm, 10 cm) and four impact azimuth

angles (0° - head-on collisions, 10°, 20°, and 40°) to provide a complete assessment of the system's ability to decelerate and remove debris objects across all relevant sizes and interaction geometries. For the 2-mm and 5-cm objects, only the head-on case was assessed.

Diam. (cm)	Alt. (km)	Incl. (°)	ΔV (m/s)	$\Delta t_{abl.}$ (s)	$T_{bef.}$ (yrs)	T_{after} (yrs)	Dist. at ablation termination (km)
0.2	800	82	661.7	4.77	3.95	~0 (<1 orbit)	22.74
1	800	82	208.4	12.42	12.58	0.006 (2 days)	22.74
		92	83.5	11.07		1.81	43.61
		102	48.4	10.05		4.81	60.63
		122	26.3	8.98		7.89	82.92
0.5	800	82	416.2	12.45	6.59	~0 (<1 orbit)	22.74
		92	162.4	11.08		0.056 (~20 days)	43.61
		102	93.5	10.05		0.64	60.63
		122	50.6	8.98		2.37	82.92
5	800	82	84.3	12.41	30.23	4.19	22.74
10	800	82	50.2	12.41	50.31	18.28	22.74
		92	20.6	11.06		35.56	43.61
		102	12.0	10.04		42.68	60.63
		122	6.5	8.98		47.76	82.92

Table 9. Simulation results for debris objects at the baseline 800-km altitude.

The parameters presented in the table are:

- Diam. (cm) – debris object diameter;
- Alt. (km) – debris object orbit altitude;
- Incl. (°) – debris object orbit inclination. Debris-laser interactions are set up such that the TCA occurs at the equator. This way, any inclination difference between the two orbits is equal to the impact azimuth angle (e.g. if the inclinations are 82° and 102°, the impact azimuth is 20°);
- ΔV (m/s) – the ΔV applied to the debris object by the laser through ablation. Reported as positive values (magnitudes), but they are all, in fact, negative (corresponding to deceleration/orbit lowering);
- $\Delta t_{abl.}$ (s) – the duration of the ablative interaction;
- T_{bef} (yrs) – the initial orbit lifetime of the unperturbed debris object, in years;
- T_{after} (yrs) – the lifetime of the perturbed debris object, after deceleration through laser ablation;
- Dist. at termination (km) – the distance between the laser satellite and the debris object at the point where any of the termination conditions forces the ablative interaction to stop and the laser to be turned off.

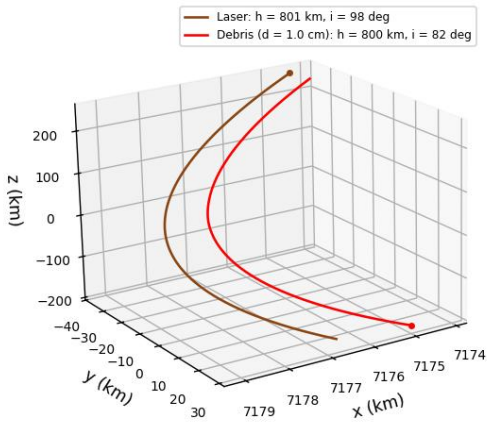

Figure 7. Simulated orbits of the laser satellite and debris object. Head-on collision case, d = 1 cm.

The results show a very good performance of the system in performing debris removal, especially for objects approaching head-on and from azimuths of up to 20°. The smaller objects (5 mm and 1 cm), which are much more abundant, can be de-orbited almost instantly from one interaction for head-on geometries. For azimuths of up to 20°, their lifetime is reduced from above to below the 5-year rule.

For the largest targeted objects (10 cm), there is still a significant lifetime reduction from 50 to 18 years in head-on interactions, from 50 to 36 years at azimuth differences of 10°, and a more modest 8-year lifetime reduction for 20° azimuths.

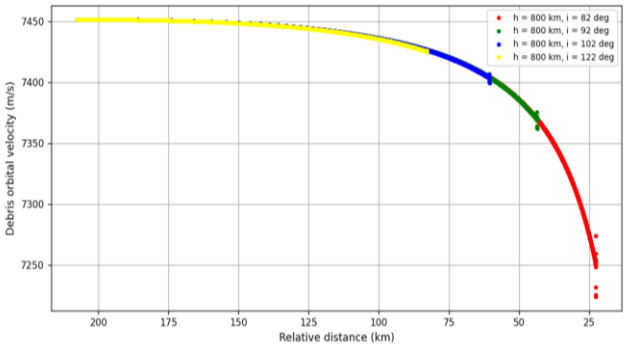

Figure 8. Orbital velocity change for the d = 1 cm debris object.

b) Debris objects at different altitudes

The second case that was analysed looked at interactions with debris objects orbiting at different altitudes than the laser system. We assumed altitude differences of ±10 km from the nominal 800-km altitude. For lower differences, the lifetime reductions should be higher.

Diam. (cm)	**Alt. (km)**	**Incl. (°)**	**ΔV (m/s)**	**$\Delta t_{abl.}$ (s)**	**$T_{bef.}$ (yrs)**	**T_{after} (yrs)**	**Dist. at ablation termination (km)**
1	810	82	45.7	9.81	13.61	5.81	61.98
		92	41.5	9.62		6.29	65.33
		102	33.7	9.23		7.32	72.87
		122	22.3	8.58		9.28	88.76
1	790	82	37.7	9.37	11.41	5.93	68.54
		92	35.4	9.25		6.19	70.85
		102	30.40	8.99		6.79	76.48
		122	21.7	8.51		8.04	89.69

Table 10. Simulation results for debris objects orbiting at different altitudes than the baseline.

Once more, the most effective lifetime reductions appear in the case of lower-azimuth interactions. At any altitude in the orbital shell, for head-on and ±10° azimuth encounters, the object's lifetime is reduced to below 6.3 years. For the 20° and 40° azimuth angles, the lifetime reductions are still of several years, from just 9-10 seconds of total ablation time.

The results are encouraging, given that about 30% of the encountered objects are expected to come from azimuths ±10°, 50% of the objects from azimuths ±20°, and 70% from azimuth angles ±40°.

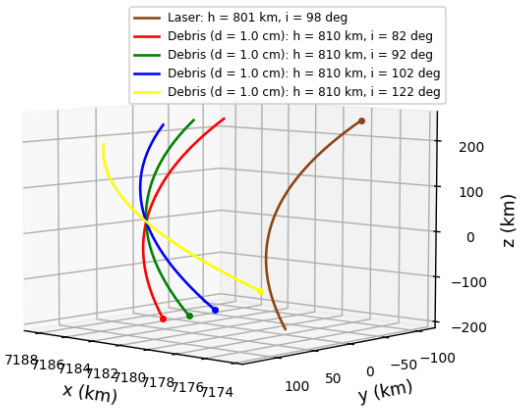

Figure 9. Simulated orbits of the laser satellite and debris objects. The debris objects orbit at a different altitude (810 km) than the laser. For d = 1 cm and all interaction geometries.

The system can therefore target objects at different altitudes, and continue to decelerate them through ablation as it lowers their orbit and they approach the nominal 800-km altitude.

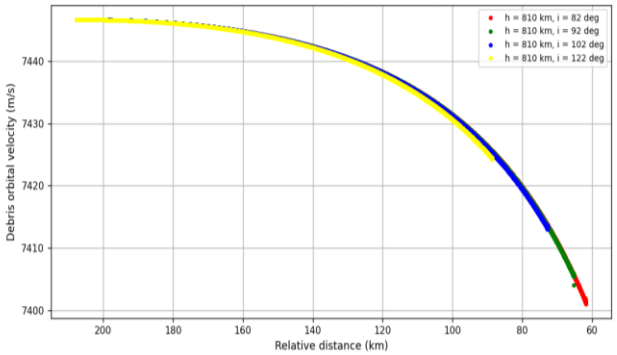

Figure 10. Orbital velocity change for the d = 1 cm object and h = 810 km.

IV. Satellite Subsystem Sizing

A. EPS

The laser sends pulses of 80 J at a repetition rate of 75 Hz. This requires an optical power of 6.0 kW. An electrical-to-optical power efficiency of 32% was assumed, meaning that the EPS needs to supply the laser system with 18.75 kW of electrical power during peak consumption, i.e. during the laser pulse firing. From the simulation results, the longest ablation duration to de-orbit one object is equal to 12.45 seconds, for the head-on impact case.

This implies that a maximum total energy of 64.84 Wh is required to ablate one object. This is equal to the maximum total energy that needs to be drawn from the storage system. We assume a 50% beginning-of-life (BOL) depth of discharge (DoD) and an energy density of the batteries of 338 Wh/kg, corresponding to modern 4680 Li-Ion cells [13]. This implies an equivalent battery capacity of 129.68 Wh, and a total battery mass of 384 grams.

The electrical energy that can be supplied by solar arrays of area A_{SA} and cell efficiency η_{SC} in time interval Δt is:

$$E = \Phi_{\odot} \cdot A_{SA} \cdot \eta_{SC} \cdot \Delta t \qquad (12)$$

where $\Phi_{\odot} = 1372 \frac{W}{m^2}$ is the total solar irradiance at 1 AU. Therefore, to fully replenish the batteries in $\Delta t = 14.6\, min$ (the expected interaction rate, as discussed below), a solar array of area $A_{SA} = 0.65\, m^2$ utilizing cells of 30% efficiency is required. Assuming that 70% of the total solar panel area can be filled with functional solar cells, solar panels of $A_{SP} = 0.92\, m^2$ need to be installed on each laser firing spacecraft.

Below, we summarise the parameters required to satisfy the electrical power demands of the payload.

B. AOCS

The successful detection, tracking, and laser ablation of the debris objects rely on precise determination and control of the spacecraft's attitude, in addition to reliable knowledge and control of each spacecraft's position such that the debris object always lies at the focal point of the laser optics.

Initially, the chief spacecraft detects an object with a positioning accuracy of 35.24 arcsec, or 79.5 m at 465 km range. The object's location and trajectory are transmitted to the deputy satellites via the ISL, at which point their AOCS must steer the tracking telescopes towards the object. The tracking optical systems have a narrow FOV of 3.61 arcmin, or 488 m at 465 km range. To make sure the target is within their FOV, the AOCS must provide a pointing accuracy of (3.61 / 2) arcmin – 35.24 arcsec = 0.0203°, or 1.22 arcmin.

As the object moves across the sky with angular velocity ω, the telescope must rotate to follow it at an equal slew rate. We assume a maximum achievable slew rate of 2°/s [17].

The moment of inertia (MoI) is estimated assuming a uniform cube-like structure. For a 500 kg satellite with dimensions ~1.2x1.2x1.2 m, the MoI about each axis is approximately:

$$I = \frac{1}{6} m L^2 \approx 120\, kg\, m^2 \qquad (13)$$

The torque required for slewing is given by:

$$T = I \cdot \alpha \qquad (14)$$

where α is the angular acceleration. The 2°/s slew rate is expected to be reached after a minimum of 5 seconds, thus the highest angular acceleration can be $\alpha = 0.4°/s^2 = 0.007\, rad/s^2$. The required torque is T = 0.84 Nm. We estimate a momentum storage of $H = I\,\omega = 4.19\, Nms$.

Once the object is successfully tracked, the laser system requires a better pointing accuracy to be able to place the laser spot on the debris object (covering the entire debris projected surface area) and keep it focused there. At the furthest range where ablation starts occurring (i.e. of around 200 km), the laser spot diameter is equal to 33.5 cm. Given that the largest targeted objects are of 10 cm in diameter, the required pointing accuracy is equal to (33.5 – 10)/2 = 11.75 cm. Converting it to an angular diameter yields a pointing accuracy of $(3.37 \times 10^{-5})° = 0.12\, arcsec$ during laser ablation.

Lastly, the AOCS must ensure that the relative position of each laser satellite with respect to the incoming object is controlled to within a certain threshold, otherwise the object would fall out of focus and the imparted fluence would decrease significantly.

The beam spread due to laser divergence is given by [13]:

$$w(R) = w_0 + R\,tan\left(\frac{M^2\lambda}{2\pi w_0}\right) \quad (15)$$

Here, w_0 is the beam radius at the focal plane, and R is the distance from the focal plane to the laser beam of radius $w(R)$.

The fluence on the target decreases with the beam radius squared. This effect will be most significant when the target is closest and a change in the focal plane position results in the greatest spot diameter change. When the focal plane lies at a range of 23 km, the spot radius is equal to 1.93 cm and the fluence on the target is of roughly 478.5 kJ/m^2. Shifting the focal plane by 1 km results in a diverging beam of radius 2.01 cm and a fluence less than 10% lower than the original one. Across all laser-target ranges, this represents the maximum fractional difference between the computed fluences and the ones arising due to uncertainties in every laser satellite's position of up to 1 km, or due to uncertainties in the along-track (longitudinal) position of the approaching debris object. This positioning accuracy is well within the current capabilities of space-rated navigation sensors such as GNSS receivers.

C. Thermal control

The main challenge for the thermal control subsystem is to dissipate the excess heat generated during laser system operations. With a 6.0 kW optical power requirement for ablation and a 32% electrical-to-optical efficiency, the power draw of the laser system is of 18.75 kW. Making the conservative estimate that all the additional power must be rejected as waste heat, we can estimate the required radiator area from the heat balance equation:

$$P_{excess\ laser} = \epsilon\,\sigma\,A_{rad.}\,T^4 \quad (16)$$

where ϵ is the radiator emissivity, $\sigma = 5.67 \times 10^{-8}\mathrm{Wm^{-2}K^{-4}}$ is the Stefan-Boltzmann constant, $A_{rad.}$ is the total surface area of the radiators, and T is the maximum temperature to which the radiators will be kept. The radiators will be coated in AZ-93 white paint, which has a high emissivity of 91% and a low absorptivity of incident sunlight, of 14-16% [23]. With $P_{excess\ laser} = 12.75\,kW$ and an operational temperature maintained at $T = 303\,K$, a radiator area of $A_{rad.} = 29.3\,m^2$ is obtained. This is an exigent requirement that can only be fulfilled by using deployable radiator panels extending away from the spacecraft's main body. Assuming a specific mass of 0.3 kg/m^2, the total radiator mass is 8.8 kg. Alternatively, active cooling technologies should be investigated to decrease the amount of waste heat that needs to be radiated away passively, if this requirement proves to be too restrictive for the proposed system.

However, the above assumes that excess heat must be rejected continuously by the radiators, even though the 12.75 kW are accumulated over only 12.45 seconds at most at a time. Another option that can be investigated is using Phase Change Materials to collect the amount of excess heat accumulated during an ablative interaction, thus allowing the radiators to dissipate it later.

In this case, 158.74 kJ of excess heat are accumulated during the 12.45 seconds of maximum ablation time. Since the expected encounter rate was estimated as 14.6 minutes, we can assume the heat can be disposed of over 12 minutes to allow for margin (if any two objects are encountered at a higher rate and the system is not ready to ablate it, it can choose to wait until the next encounter). Hence, the average power to be continuously radiated away equals 220.5 W. Using this value once again in the heat balance equation, we obtain a radiator area of $A_{rad.} = 0.51\,m^2$, with a total mass of 0.15 kg.

To transport the heat away from the mirrors and laser system towards the deployable radiators, variable-conductance heat pipes can be used. This is because the amount of waste heat that needs to be dissipated varies significantly across the foreseen mission operations (e.g. between laser ablation mode and stand-by mode for the deputies, when the chief scans the sky for new debris objects).

V. Autonomous Navigation

Two areas are of interest with regard to the autonomous navigation of the Olaf service: the position estimation of each satellite (absolute positioning accuracy at individual level and relative positioning accuracy at swarm level), and the formation keeping control performance (mainly the inter-satellite distances between which the members can be kept while still providing sufficient laser ablation performance and ensuring collision avoidance).

A. Requirements

The absolute positioning accuracy requirement is 1 m (3D RMS) for each satellite. This is because by shifting the focal plane by 1 m when the debris is 20 km away results in a fluence which is 99.9% as high as the optimal one. This positioning accuracy is well within the current capabilities of space-rated navigation sensors such as GNSS receivers. The OrbFix GNSS-based PNT device developed by RISE can achieve a dm-level 3D RMS positioning accuracy in LEO and is selected as the baseline option to be employed on all of the swarm satellites.

In terms of the formation keeping requirements of the mission, two aspects need to be addressed: the performance loss with respect to having all satellites at the leader's location (i.e. the 'ideal' case in which we have a virtual large laser system firing from the same location) and the collision avoidance necessity between swarm members. In a real-world scenario, the chief would monitor the probability of collision between any two swarm members and ensure it is kept below 10^{-4}. In this work, a simplified approach is adopted, in which we require that the distance between any two satellites stays above 1 km at all times (also noting the positioning accuracy requirement).

For the fluence loss due to the formation geometry, the worst-case scenario is that in which the debris object is closest to the formation. Here, the angle between the debris-chief line of sight and debris-deputy line of sight is greatest. In addition, the fluence imparted on the debris is highest, as the fluence increases with the laser-debris distance squared.

From the simulations, the closest debris-formation distance at which ablation can still occur is of >20 km. For a chief-deputy distance (i.e. circle radius) of 6.5 km, the deputy-debris distance becomes 21.03 km. The fluence imparted on the debris at 21 km range equals 90.7% of that imparted at 20-km range. This justifies our selection of the 90% efficiency factor due to formation geometry losses, and shows that it is a conservative estimate, because the imparted fluence would be higher than 90% of the optimum when the debris is further away from the formation.

To conclude, the circular formation's radius must be kept below 6.5 km at all times, whilst ensuring that no two satellites approach to within 1 km from one another. As is shown in the formation flying simulations below, a 2-km initial radius for the circular formation can satisfy this requirement, together with additional considerations.

B. High-level relative navigation architecture

A combined GNSS + RF-ranging architecture was selected as the baseline for the mission. Each spacecraft performs GNSS-based absolute navigation. In addition, all spacecraft are equipped with radio-frequency (RF) inter-satellite links capable of performing pairwise ranging measurements. These measurements are used as secondary relative constraints and are transmitted to the chief spacecraft, which executes a centralized Extended Kalman Filter (EKF) to estimate the relative orbital states of all deputy spacecraft simultaneously.

RF measurements are also used to ensure a reliable relative state solution under GNSS degradation. Unlike GNSS, RF ranging does not provide absolute positioning but improves the relative state estimation of the formation. With seven deputy spacecraft, the total number of RF measurements is (assuming connections between all pairs of members in the formation):

$$N_{tot} = \frac{7 \times 8}{2} = 28$$

The filter state vector is defined as:

$$x = [\delta\alpha_1^T \quad \delta\alpha_2^T \quad \cdots \quad \delta\alpha_7^T]^T \tag{17}$$

where $\delta\alpha_n^T$ is the relative orbital element state vector of deputy n, with respect to the chief. The resulting filter dimension is therefore 7 x 6 = 42.

By continuously fusing dynamic predictions with real sensor measurements, the EKF produces statistically optimal relative state estimates in the minimum mean-square error sense under Gaussian noise assumptions. Thus, the use of the sensor fusion algorithm significantly improves the relative navigation accuracy, system robustness to measurement outages, and long-term estimation stability.

VI. Formation Keeping Modelling

A. Theoretical approach

D'Amico [24] has introduced a full GNC solution for formation flying of LEO satellites. A relative inclination/eccentricity separation is proposed, where the formation is given by the following elements for J2 stability:

$$\delta\alpha = \begin{bmatrix} \delta a \\ \delta\lambda \\ \delta e_x \\ \delta e_y \\ \delta i_x \\ \delta i_y \end{bmatrix} = \begin{bmatrix} 0 \\ 0 \\ 0 \\ \pm\delta e_{nom} \\ 0 \\ \pm\delta i_{nom} \end{bmatrix} \tag{18}$$

where δe_{nom} and δi_{nom} are chosen such that the minimum inter-satellite distance is equal to $a \min\{\delta e_{nom}, \delta i_{nom}\}$. The orbital element differences $\delta\alpha$ are related to the set of mean orbital elements by the following relations:

$$\delta\alpha = \begin{bmatrix} \delta a \\ \delta\lambda \\ \delta e_x \\ \delta e_y \\ \delta i_x \\ \delta i_y \end{bmatrix} = \begin{bmatrix} \frac{a_d - a}{a} \\ (u_d - u) + (\Omega_d - \Omega)\cos i \\ e_{x_d} - e_x \\ e_{y_d} - e_y \\ i_d - i \\ (\Omega_d - \Omega)\sin i \end{bmatrix} \tag{19}$$

The elements that have the *d* subscript refer to a deputy satellite, while the ones without subscript refer to the chief satellite. The relationship between the modified set of orbital elements and the classical one is:

$$\alpha = \begin{bmatrix} a \\ u \\ e_x \\ e_y \\ i \\ \Omega \end{bmatrix} = \begin{bmatrix} a \\ \omega + M \\ e\cos\omega \\ e\sin\omega \\ i \\ \Omega \end{bmatrix} \tag{20}$$

The suggested elements for the maximisation of passive formation keeping only allow for a maximum of 4 deputy satellites to be used, which is less than we require. As such, a softer (and more expensive) formation keeping condition is chosen: to ensure that the minimum distance formula holds and the formation is bounded in terms of inter-satellite distances, the eccentricity and inclination vectors need to be parallel or antiparallel. This allows a simple separation scheme for n deputy satellites based on vector phasing:

$$\begin{bmatrix} \delta e_x \\ \delta e_y \\ \delta i_x \\ \delta i_y \end{bmatrix} = \begin{bmatrix} \delta e \cos\left(\frac{2\pi}{n} + \frac{\pi}{2}\right) \\ \delta e \sin\left(\frac{2\pi}{n} + \frac{\pi}{2}\right) \\ \delta i \cos\left(\frac{2\pi}{n} + \frac{\pi}{2}\right) \\ \delta i \sin\left(\frac{2\pi}{n} + \frac{\pi}{2}\right) \end{bmatrix} \tag{21}$$

The minimum distance between any two deputy satellites will be given by the length of the chord between them, namely $d_{min} = 2r\sin\frac{\pi}{n}$. Using this equivalence, it is possible to use either the length of the chord or the radius of the relative orbit circle to space the satellites. For the length of the chord, $a\delta e = \frac{d_{min}}{2\sin\frac{\pi}{n}}$, resulting in $\delta e = \frac{d_{min}}{2a\sin\frac{\pi}{n}}$. δi is chosen to have the same value δe so the relative distance oscillations are identical in amplitude.

The bounded, centred relative motion necessary conditions in absence of J2 are: $\delta a = 0$ and $\delta\lambda = 0$.

The condition for a closed relative orbit around an oblate Earth is given to first order by:

$$\frac{J_2 R_E^2}{2a^2\eta^4}\sin(2i)\,\delta i_x + \frac{1}{7}\delta a = 0 \quad (22)$$

These conditions cannot be satisfied at the same time, as δi_x is not 0 for the given separation scheme unless the number of satellites is less than 4 (for fewer than 4 satellites a different separation scheme can be used in which they are not equidistant but δi_x is 0). As such, the $\delta a = 0$ condition is dropped, and it is instead computed based on δi_x.

The outlined constraints allow a complete determination of the relative orbital elements for the deputy satellites.

The passive stability of the formation does not last sufficiently for the mission, so a 7-day cycle of correction ΔVs is used to maintain it. The computation of the ΔV is done based on D'Amico's framework [24] but using a slightly different approach. Every 7 days, new ideal relative orbital elements are computed using the process described previously with respect to the chief satellite. The ideal relative orbital elements are then converted into the absolute Brouwer mean orbital elements (with both short-term and long-term variations removed). These are used to compute a new set of relative orbital elements between the real Brouwer elements of each deputy and the ideal ones (using the real satellite's elements as a virtual chief and the ideal ones as a virtual deputy). Finally, D'Amico's relations between the ΔV and relative orbital elements allow for the computation of 3 correction manoeuvres (2 in-plane and 1 out-of-plane) and their timings.

For the in-plane correction manoeuvre pair, D'Amico gives the following tangential and radial ΔVs [24]:

$$\delta v_{t_1} = \frac{na}{4}[\delta a + \delta e\cos(u_{M_1} - \xi)] - \frac{na}{4}\chi\left[\frac{\delta\lambda}{2} + \delta e\sin(u_{M_1} - \xi)\right] \quad (23)$$

$$\delta v_{r_1} = \frac{na}{2}\left[-\frac{\delta\lambda}{2} + \delta e\sin(u_{M_1} - \xi)\right] - \frac{na}{2}\chi[\delta a - \delta e\cos(u_{M_1} - \xi)] \quad (24)$$

$$\delta v_{t_2} = \frac{na}{4}[\delta a - \delta e\cos(u_{M_1} - \xi)] + \frac{na}{4}\chi\left[\frac{\delta\lambda}{2} + \delta e\sin(u_{M_1} - \xi)\right] \quad (25)$$

$$\delta v_{r_2} = \frac{na}{2}\left[-\frac{\delta\lambda}{2} - \delta e\sin(u_{M_1} - \xi)\right] + \frac{na}{2}\chi[\delta a - \delta e\cos(u_{M_1} - \xi)] \quad (26)$$

Where n is the mean motion of the real deputy, $\chi = \frac{\sin(u_{M_2} - u_{M_1})}{\cos(u_{M_2} - u_{M_1}) - 1}$ and $\xi = \text{atan2}(\delta e_y, \delta e_x)$. Focusing on the assessment of feasibility, we have chosen $u_{M_2} - u_{M_1} = \pi$ (resulting in $\chi = 0$) and $u_{M_1} = \xi$ (resulting in the δe terms only contributing to the tangential components, which are half as costly).

For the out-of-plane correction we utilize a single normal ΔV:

$$\delta v_{n_3} = na\delta i \quad (27)$$

$$u_{M_3} = \text{atan2}(\delta i_y, \delta i_x) \quad (28)$$

The 3 mean arguments of latitude for the manoeuvres get translated to the [0, 3π) interval (u_{M_1} and u_{M_3} are in [0, 2π)). The time to execution is then computed based on the real mean motion of the deputy at the time of computation, and converted to the nearest integer simulation step. As the simulation step is 60 s, some error in the timing is expected to occur, but given the nominal orbital period of around 6000 s, the achieved accuracy will be enough to maintain the formation.

B. Simulation setup

This section presents the simulation results for a 1-year simulation using 8 identical satellites (1 chief and 7 deputies) with the same parametrisations as in Table 6.

The simulations were run for a duration of one year, at a step size of 60 s. The GMAT R2025a software was used for orbital propagation, using the EGM-96 gravity model of degree and order 60, the Jacchia-Roberts atmospheric model, the Moon and the Sun as gravitational point masses, and an average solar flux of 190 sfu.

The initial conditions of the 8 spacecraft are captured in the table below. The chief satellite is satellite number 1. Note that the orbital elements provided are Brouwer mean elements with both long- and short-term variations removed. The initial elements correspond to an approximately circular orbit of 800 km altitude with the deputy satellites spread in a circle of approximately 2 km around the chief and having 1.75 km separation distance between two deputies closest to each other.

Satellite number	Semi-major Axis [km]	Eccentricity [-]	Inclination [deg]	Right Ascension of the Ascending Node [deg]	Argument of Perigee [deg]	Mean Anomaly [deg]
1	7178.09997	2.4383e-08	97.999	7.4099e-08	88.03182	271.96818
2	7178.09997	0.00028	97.999	0.01626	89.99978	270.00249
3	7178.09866	0.00028	97.987	0.01014	141.42358	218.57784
4	7178.09834	0.00028	97.984	359.99638	192.85114	167.14836
5	7178.09924	0.00028	97.993	359.98535	244.28320	115.71476

6	7178.10068	0.00028	98.007	359.98535	295.71716	64.28080
7	7178.10158	0.00028	98.016	359.99638	347.14896	12.85054
8	7178.10126	0.00028	98.013	0.01014	38.57615	321.42526

Table 11. Initial orbit elements for the formation keeping simulations.

C. Simulation results with 7-day maintenace period

For this simulation, the formation maintenance manoeuvres were computed once every 7 days and performed within 1-2 orbits of computation, depending on the required mean argument of latitude. The distances in km between each deputy satellite (named Olaf 2-8) and the chief (Olaf 1) were obtained.

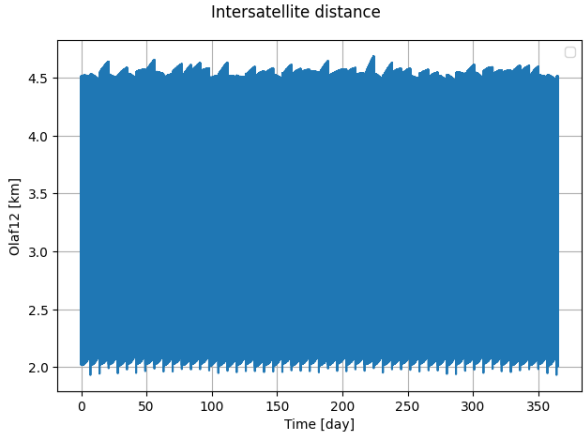

Figure 11: Distance between Olaf 2 and Olaf 1.

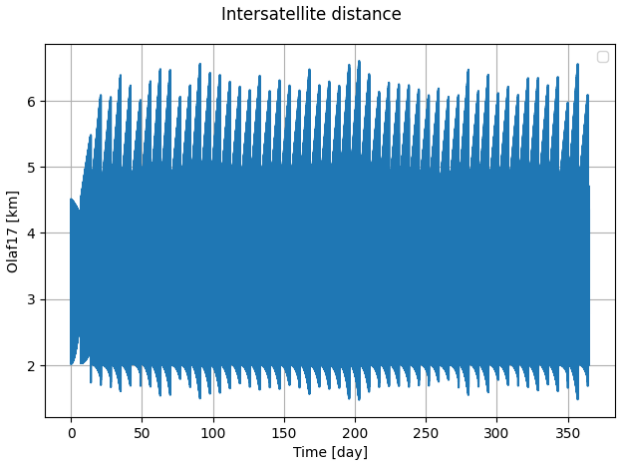

Figure 12: Distance between Olaf 7 and Olaf 1.

The minimum and maximum distances between any two deputies are 1.04 km and 11.41 km. The inter-satellite distance plots for the respective deputies are presented in the two figures below.

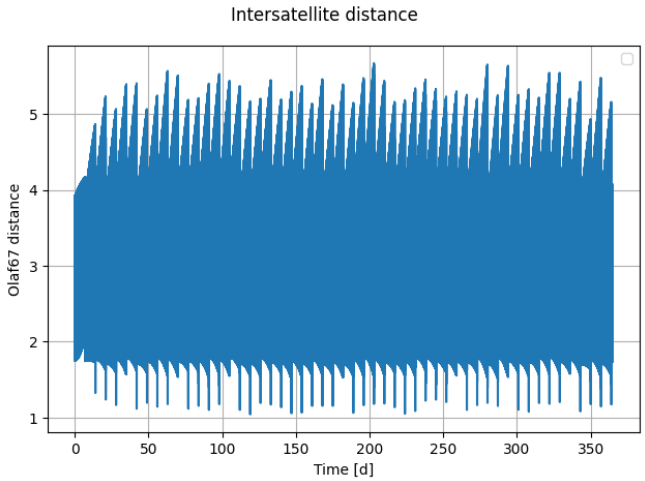

Figure 13: Distance between Olaf 6 and Olaf 7. Minimum ISD between any two deputies.

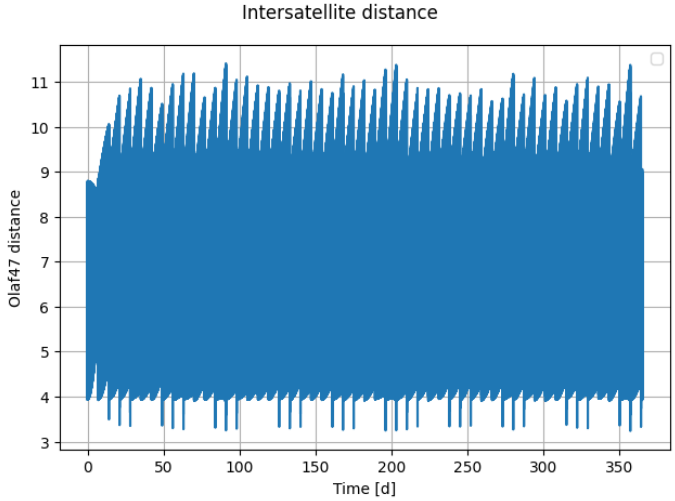

Figure 14: Distance between Olaf 4 and Olaf 7. Maximum ISD between any two deputies.

The total ΔV budget required to maintain the formation for the year is presented in the following table.

Satellite number	ΔV consumed [m/s]
1	0
2	48.44
3	131.07
4	121.71
5	69.96
6	106.00
7	186.93
8	123.04

Table 12: Delta-V budget for 1 year per spacecraft. Chief = sat. no. 1. Deputies = sats. no. 2-8. For 7-day maintenance period.

The variation of the ΔV budget between the deputies is mainly given by the proximity of their inclination and eccentricity vectors to the safe condition of $\delta e_x = \delta i_x = 0$.

This leads to an interval of variation of the ΔV magnitude that might be difficult to execute with uniformly-sized thrusters. However, delaying the manoeuvre until a significant correction needs to be performed has a non-linear impact in both fuel cost and inter-satellite distance. One potential solution to this problem is the use of electric propulsion to achieve the corrections, as that would be able to deliver both small and large amounts of ΔV (over a longer period). This would need to be evaluated against the availability requirements of the mission or allow for thrust vectoring.

In conclusion, formation keeping is feasible under the presented assumptions and formation geometry. Starting from a roughly circular formation of radius 2 km, with the chief at the centre, and ensuring that corrective ΔVs are applied once every 7 days, the inter-satellite distances can be maintained between 1 and 11.5 km throughout the mission lifetime. These values are consistent with the navigation requirements, stating that ISDs must be kept above 1 km to ensure collision avoidance, and that the circle radius must be kept below 6.5 km to ensure enough fluence can be imparted on the incoming debris object by each laser satellite (assuming, in the worst case, that the diameter becomes 11.41 km, the radius still falls below 6.5 km). The annual ΔVs that must be applied to each deputy satellite range between 48 and 187 m/s. While demanding, these values can be reached using ion thrusters/electric propulsion systems.

VII. Economic Considerations

A. Space debris environment

To assess the system's ability to perform debris removal, the total number of expected interactions was estimated. The simulations showed that the proposed laser system is effective for objects orbiting in a ±10 km altitude range, thus the spatial density of RSOs between 790 and 810 km was assessed.

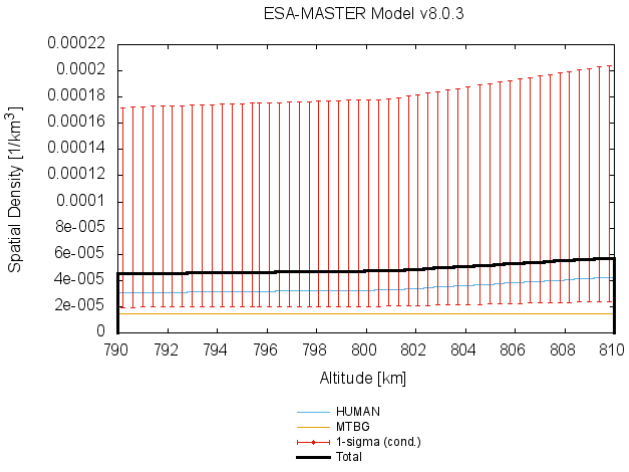

Figure 15. Spatial density of 0.1-10 cm objects in the 790-810 km altitude range.

MASTER computed an average density of 4.41 x 10^{-5} objects/km^3. We approximate the volume of space that these objects inhabit as a spherical shell extending from 790 km to 810 km above the Earth's surface. This volume is equal to:

$$V_{shell} = \frac{4\pi}{3}((R_E + 810km)^3 - (R_E + 790km)^3) = 1.29 \times 10^{10}\ km^3 \quad (29)$$

Thus, we expect to find a number of 568890 debris objects within this spherical shell, at any moment of time (evaluated at the epoch at which the spatial density was computed, i.e. 1st January 2030).

The most significant debris lifetime reductions were obtained for those objects approaching to within about 75 km or less of the laser swarm at the TCA. For this rough order of magnitude estimate, we can use the conservative assumption that only those objects are ablated and removed from orbit (or their lifetime is significantly reduced).

For a debris object to be at 75 km or less from the laser at the TCA, it must be located within a cylindrical tube whose base is centred at the laser swarm, with a 10-km radius and a 75-km height (i.e. length along the projected trajectory of the laser swarm satellites). This ensures we limit ourselves to objects within the 790-810 km shell. The furthest diagonal distance from the lasers along the cylinder is 75.66 km, about the same as the cylinder height.

The volume of this cylinder is equal to $V_{cylinder} = \pi(10\ km)^2(75\ km) = 23562\ km^3$. Therefore, the probability of finding a debris object within this cylindrical tube at any time t equals:

$$P_{enc.\,at\,t} = \frac{V_{cylinder}}{V_{spherical\ shell}} = 1.827 \times 10^{-6} \quad (30)$$

The orbital period of the laser satellites at 800 km altitude is 6052 seconds (100.9 minutes). The probability of encountering a debris object over one orbit is:

$$P_{enc.\,per\,orbit} = 6052 \times 1.827 \times 10^{-6} = 0.011054 \quad (31)$$

Assuming the volume of the orbital tube to be approximated by a torus of radius R = R_E + 800 km, and whose radius of the revolving circle is r = 10 km, we compute:

$$V_{orbit\ tube} = 2\pi^2 Rr^2 = 2\pi^2(R_E + 800\ km)(10\ km)^2 = 1.417 \times 10^7\ km^3 \quad (32)$$

Thus, we expect a number of $P_{enc.\,per\,orbit} \times \rho_{debris\ obj.\,790-810\ km} \times V_{orbit\ tube} = 6.9076$ objects to be encountered per orbit within the desired interaction tube as the laser swarm's trajectory is propagated in time.

There are 14.28 orbital revolutions per day, or 5215.8 revolutions per year. This brings the expected number of encounters per year to 36029. Over a 5-year ADR mission, 180144 objects are expected to be encountered by the laser swarm.

As described in the sections above, the fraction of debris objects our system can detect and interact with come from azimuth angles ±40°, so from inclinations 42°-122° (i.e. ±40° from the head-on 82° inclination case). These represent 70.7% of all objects encountered by the laser swarm during the mission lifetime, i.e. 127362 objects.

Since the proposed system uses optical telescopes in the visible spectrum for both detection and tracking, the debris objects have to be sunlit for the system to interact with them.

The baseline option for the laser swarm orbit type is an 800-km dawn/dusk SSO at 98° inclination. This would ensure near-constant sunlight illumination for our system. If we point the scanning sensor away from the Sun, we expect nearly all objects to be illuminated across half a hemisphere.

For more general Sun-synchronous orbits, the number of sunlit objects encountered by the Olaf system may decrease. The eclipse durations are expected to be of at most 35 minutes per orbit for these orbit types, with periods of ~100 minutes. With this in mind, we estimate the fraction of sunlit objects to be 65% of the ones encountered over the mission lifetime.

This brings the total number of debris objects expected to be removed from orbit (or whose lifetime is significantly reduced) at 82785 over a 5-year mission, assuming we operate on a general SSO (not dawn/dusk).

The average interaction rate per orbit is estimated as 100.9 minutes / 6.9076 objects = 14.61 minutes. Thus, we expect to encounter a debris object that the laser system can ablate once every 14-15 minutes, on average.

B. Estimated cost

A preliminary iteration of the mass budget reaches between 300 and 485 kg for each satellite in the swarm.

The cost of the major system components is estimated at this stage at 4.5 million EUR for the satellite bus, 12 million EUR for the tracking telescope, 15 million EUR for the detection telescope and 35 million EUR for the laser ablation system. The launch cost for each deputy satellite is estimated at 1.8-3.0 million EUR using the SpaceX Falcon 9. The launch cost of the chief spacecraft would be 1.5 million EUR. Thus, the total launch cost of the 11 satellites is estimated at 31.5 million EUR. This assumes a cost of 6000 EUR/kg launched, consistent with SpaceX prices for launches of 300-500 kg spacecraft in rideshare mode.

This brings the estimated total cost of the space segment of the Olaf service to ~430 million EUR (with added margin, including launch), pointing to a cost per de-orbited debris object of 3400-5000 EUR, depending on the type of Sun-synchronous orbit the system is launched into (dawn/dusk or not).

We mention that these figures are indicative only and no attempt at a detailed cost budget analysis was made. This is because the main technologies enabling the successful completion of this mission will still require significant R&D efforts to bring them to flight readiness in the proposed configuration, thus many unknowns remain. In particular, high-accuracy real-time orbit determination by space-based SSA sensors and space-based laser ablation at the peak power levels assumed in all ADR studies are yet to be proven.

VIII. CONCLUSION

In this work, we have proposed an architecture for the Olaf service that aims to remove large populations of small debris objects in LEO using space-based laser ablation.

The ADR system is based on a swarm of 7 deputy satellites and a chief satellite. Using 355 nm Nd:YAG lasers, the swarm fires 80 J pulses at a repetition frequency of 75 Hz on approaching debris objects, ablating them and accelerating their de-orbiting process. Significant lifetime reductions were obtained for most interaction geometries, with near-instant de-orbiting for smaller objects (1 mm – 1 cm) and reductions to below 5 years from initial lifetimes of decades, for objects up to 5 cm in diameter.

While the deputies utilise 60-cm f/3.25 telescope for precision tracking of debris, as well as dynamic laser beam focusing at the required ranges, the chief satellite uses a 40°-FOV 40-cm f/1.2 telescope to detect incoming objects from a maximum distance of 4871 km (for a 10 cm debris). The chief is also responsible for the relative navigation of the swarm, coordinating the deputies via the ISL. In addition, it ensures the TT&C link with the ground.

Formation flying simulations showed that formation control is feasible by performing a ΔV manoeuvre every 7 days. The ΔV budget was found to require between 48 and 187 m/s annually, depending on the satellite. The mass of each satellite is in the order of 300-500 kg, with a total estimated cost for the system of less than 430 million EUR, including launch.

Overall, the Olaf service has been shown to be feasible in terms of reducing the small (1 mm – 10 cm) space debris population, being capable of de-orbiting up to 130,000 objects when placed on a dawn/dusk 800-km SSO, at an estimated cost of €3400/object.

In addition to debris removal, the Olaf service can be used for space-based SSA, detecting new objects and supplementing the space debris catalogues. Another possible use case is the provision of conjunction warnings based on small debris objects (undetectable from the ground) to interested satellite operators.

To bring the proposed system towards successful implementation, the detection, tracking, and laser ablation payloads would require TRL raising through extensive R&D efforts. At theoretical level, directions of future study include the detailed description, mathematical framework, and modelling of the relative state estimation task performed by the chief spacecraft, the verification of the laser ablation performance under interactions with a numerous debris population (e.g. generated from the NASA breakup model) to assess the percentage of favourable geometries under which significant lifetime reductions are achieved, and the development of an end-to-end simulation incorporating all tasks that the laser swarm must complete.

IX. ACKNOWLEDGEMENTS

The authors would like to thank Daniele Valentino Bella, Stefano Binda, and Eleftherios Plakidis of the European Space Agency for their technical advice and support offered throughout the various stages of this project.

REFERENCES

[1] ESA Space Debris Office, "ESA's Annual Space Environment Report," European Space Agency, No. GEN-DB-LOG-00288-OPS-SD, 2026.

[2] ESOC, "MASTER. Meteroid And Space debris Terrestrial Environment Reference," European Space Agency, 2026. [Online]. Available: https://sdup.esoc.esa.int/master/. [Accessed 24 May 2026].

[3] K. Donald J. and C.-P. Burton G., "Collision frequency of artificial satellites: The creation of a debris belt," Journal of Geophysical Research: Space Physics, vol. 83, no. A6, pp. 2637-2646, 1978.

[4] A. Horstmann, A. Manis, V. Braun, M. Matney, A. Vavrin, D. Gates, J. Seago, P. Anzmeador, C. Wiedemann and S. Lemmens, "Flux Comparison of Master-8 And Ordem 3.1 Modelled Space Debris Population," in 8th European Conference on Space Debris, Darmstadt, Germany, 2021.

[5] G. Drolshagen, "Impact effects from small size meteoroids and space debris," Advances in Space Research, vol. 41, no. 7, pp. 1123-1131, 2008.

[6] H. Schaub, L. E. Jasper, P. V. Anderson and D. S. McKnight, "Cost and risk assessment for spacecraft operation decisions caused by the space debris environment," Acta Astronautica, vol. 113, pp. 66-79, 2015.

[7] ESA Space Debris Mitigation Working Group, "ESA Space Debris Mitigation Requirements," European Space Agency, ESSB-ST-U-007 Issue 1, 2023.

[8] S. Minghe, G. Jian and G. Eberhard, "Review and comparison of active space debris capturing and removal methods," Progress in Aerospace Sciences, vol. 80, pp. 18-32, 2016.

[9] W. O. Schall., "Orbital debris removal by laser radiation," Acta Astronautica, vol. 24, pp. 343-351, 1991.

[10] C. R. Phipps, "L'ADROIT – A spaceborne ultraviolet laser system for space debris clearing," Acta Astronautica, vol. 104, no. 1, pp. 243-255, 2014.

[11] L. Pieters and R. Noomen, "Simulating arbitrary interactions between small-scale space debris and a space-based pulsed laser system," Advances in Space Research, vol. 72, no. 7, pp. 2778-2885, 2023.

[12] E. Bögel, H. Buurmeijer, L. Veithen, F. Meijering, G. A. Teixeira, D. Rehling, J. Fernánde, P. van Wolfswinkel, N. Zandvliet and S. J., "Feasibility Analysis of Small-Size Space Debris Removal in Low-Earth Orbit by Space-Based Laser Ablation," in 29th International Symposium on Space Flight Dynamics, Darmstadt, Germany, 2024.

[13] L. Walker and M. Vasile, "Space debris remediation using space-based lasers," Advances in Space Research, vol. 72, pp. 2786-2800, 2023.

[14] I. Fodde, W. Boumchita, A. Kaluthantrige, V. Savitski, M. Vasile and J. Feng, "The LASERS Mission Concept for Active Debris Removal using Laser Ablation by a Swarm of CubeSats," in International Astronautical Congress 2023, Baku, Azerbaijan, 2023.

[15] M. Meftah, L. Damé, D. Bolsée, A. Hauchecorne, N. Pereira, D. Sluse, G. Cessateur, A. . Irbah, J. Bureau, M. Weber, K. Bramstedt, T. Hilbig, R. Thiéblemont, M. . Marchand, F. . Lefèvre, A. . Sarkissian and S. and Bekki, "SOLAR-ISS: A new reference spectrum based on SOLAR/SOLSPEC observations," Astronomy and Astrophysics, vol. 611, no. A1, 2018.

[16] H. Raab, "Detecting and measuring faint point sources with a CCD," Jan. 2002. [Online]. Available: https://www.researchgate.net/publication/239582814_Detecting_and_measuring_faint_point_sources_with_a_CCD. [Accessed 5 Aug. 2025].

[17] C. R. Phipps and C. Bonnal, "A spaceborne, pulsed UV laser system for re-entering or nudging LEO debris, and re-orbiting GEO debris," Acta Astronautica, vol. 118, no. 12, pp. 224-236, 2016.

[18] C. R. Phipps, "Laser impulse coupling at 130 fs," Applied Surface Science, vol. 252, no. 13, pp. 4838-4844, 2006.

[19] K. Tsuno, S. Wada, T. Ogawa, N. Saito, T. Fukushima, T. Ebisuzaki, Y. Nakamura and A. & Sasoh, "Laser ablation induced impulse study for removal of space debris mission using small satellite," Applied Physics A, vol. 128, no. 932, 2022.

[20] L. G. Jacchia, "Revised Static Models of the Thermosphere and Exosphere with Empirical Temperature Profiles," Smithsonian Astrophysical Observatory Special Report, vol. No. 332, 1971.

[21] L. Pieters, "Active small-scale space debris removal by a space-based laser. MSc Thesis," TU Delft, Delft, the Netherlands, 2020.

[22] P. D. Anz-Meador and A. E. Potter, "Density and mass distributions of orbital debris," Acta Astronautica, vol. 38, no. 12, pp. 927-936, 1996.

[23] K. Kosmo, M. Pryor, P. Lubin, G. B. Hughes, H. O'Neill, P. Meinhold, J. Suen, J. Riley, J. Griswold, B. V. Cook, I. E. Johansson, Q. Zhang, K. Walsh, C. Melis, M. B. J. Kangas, C. Motta, T. Brashears, S. Mathew and J. Bollag, "DE-STARLITE: A directed energy planetary defense mission," Nanophotonics and Macrophotonics for Space Environments VIII, vol. 9226, no. 04, 2014.

[24] S. D'Amico, "Autonomous Formation Flying in Low Earth Orbit," Technische Universiteit Delft, Delft, Netherlands, 2010.